TRANSITION IN A DISTURBED ENVIRONMENT

E. Reshotko and D.K. Paik
Case Western Reserve University
Cleveland, Ohio 44106

The title of this presentation is the title of our research grant. While transition study is the objective of the work, the results to date are principally on the properties of turbulent boundary layers at low Reynolds numbers.

EXPERIMENTAL EQUIPMENT

The work was done in a small open-return wind tunnel of poor flow quality. Furthermore its flow quality could easily be made worse. The tunnel (fig. 1) is 19.7 cm (7-3/4 in) high. The test section is about 66 cm (26 in) long. The flow velocity is of the order of 6 m/sec (20 ft/sec) so that unit Reynolds numbers are about 366 000/m (120 000/ft). The test plate spans the tunnel and fills the length of the test section. The plate leading edge is elliptical, and a small flap is attached to the downstream end of the plate to set the attachment line on the working side of the leading edge of the plate. Measurements were made over the first 18 cm (0.6 ft) downstream of the leading edge by using a translating hot-wire probe in the spanwise centerplane. No spanwise variations are measured. Length Reynolds numbers for all of the data recorded were under 75 000. Test section turbulence levels were altered by placing grids at the location ahead of the contraction indicated in figure 1. The grids used and the corresponding test-section turbulence levels are shown in figure 2.

MEAN BOUNDARY-LAYER RESULTS

The mean boundary-layer development is shown in figure 3. In the absence of a grid the growth of Re_θ (fig. 3(a)) seems to be laminar, but the values are at about twice the Blasius level for the same distance from the leading edge. With grid 1 the boundary layer starts growing at a more rapid rate (shaded points) beyond 9 cm from the leading edge. For grid 2 the more rapid growth begins at about 6 cm from the leading edge. The corresponding shape factors are shown in figure 3(b). In the absence of a grid the shape factors decrease continuously from about 2.6 to 1.9 over the range of measurement. The no-grid data are believed to be transitional for reasons to be elaborated later. With grids 1 and 2 the shaded points corresponding to the more rapid growth in momentum thickness in figure 3(a) have shape factors below 1.7 and are believed to be turbulent. For these points a shear velocity u_τ could be obtained by fitting the profiles to a law of the wall.

An example of the determination of u_τ is shown in figure 4 for the grid 2 profile at $x = 9$ cm. The law-of-the-wall expression used is the algebraic form developed by Musker (ref. 1) that includes the laminar sublayer and the buffer layer and in the log-linear region displays Coles' constants (ref. 2). By comparing the experimental points made dimensionless with different values of u_τ with the Musker curve, a value of u_τ of 0.34 m/sec (1.12 ft/sec) was chosen based primarily on the points in the near log-linear

region. A more impressive fit is shown in figure 5. To be noted in both figures 4 and 5 is the absence of a wake component to the velocity profile. This is true of all the points obtained with grids 1 and 2 that are identified as turbulent.

For the no-grid case (fig. 6) a shear velocity determination could not be made in this way as the profiles did not display law-of-the-wall similarity. Hence what is plotted is u/u_e versus y/δ. The boundary-layer thickness δ is not a measured thickness. Rather it is computed from the displacement thickness and shape factor by using the relation $\delta/\delta^* = (H + 1)/(H - 1)$. With this normalization the location where $y/\delta = 1$ corresponds to a 0.95 velocity ratio. The profiles are collapsed for $y > \delta$, while for $y < \delta$ the velocity profiles fill out with distance downstream. This supports the identification of the no-grid data as transitional.

Next, we consider the skin friction behavior of the turbulent points obtained with grids 1 and 2. Shown in figure 7 is a semilog plot of u_e/u_τ versus Re_θ. The present data are the shaded points in the lower left of the figure, which correspond to the shaded points in figure 3. The other points come from prior investigations of flat-plate turbulent boundary layers at low turbulence levels and include the Wieghardt data as reduced by Coles (ref. 3), the data of Purtell, Klebanoff, and Buckley (ref. 4), and the data of Murlis, Tsai, and Bradshaw (ref. 5). All these data at low turbulence level seem consistent with each other and with Coles' (ref. 2) model based on a diminishing wake strength as Re_θ reduces toward a value just below 500. The present data display both the level and slope for u_e/u_τ versus Re_θ of a boundary layer that has no wake strength. This is seen by comparison with the calculated curve from the Musker profile for $\pi = 0$.

In 1962, Coles (ref. 2) did allude to the reduction in wake strength and elevated skin friction to be expected with an increase in turbulence level. A more plausible physical hypothesis has been advanced by Huffman and Bradshaw (ref. 6) through their comparison of turbulent boundary layers developing under a quiescent irrotational free stream with the turbulent flow in pipes, where the turbulent core is neither quiescent nor irrotational. In the latter flow there is no observable wake; in the former there is definitely a wake component to the velocity profiles. For the turbulent boundary layer at low Reynolds numbers in quiescent environments, Huffman and Bradshaw attribute the erosion of the wake component to the increased importance of the viscous superlayer - the interface between the boundary layer and the irrotational external flow - in eroding the wake component. For external flows at elevated free-stream turbulence - by analogy to the situation in pipes - the wake component is eroded more severely if not entirely as in the present results. An attempt will be made in our future work to develop this argument further in conjunction with other data sets for turbulent boundary layers developing in disturbed streams.

DISTURBANCE FLOW RESULTS

Figures 8 and 9 show the longitudinal turbulence intensity distribution at various values of Re_θ for the grid 1 and grid 2 data, respectively. The peak value of u'/u_τ is about 2.35 to 2.4 at $y^+ = 13$. The approximate similarity shown in the figures is in good agreement with the results of Purtell et al. (ref. 4). Beyond the peak, the data points fall until they

eventually level at u_e'/u_τ corresponding to the free-stream disturbance level. Taken together with the u_e/u_τ values for these profiles, they give a measure of the free-stream disturbance level, which turns out to be about 5.5 percent for grid 1 and 6.7 percent for grid 2. The Purtell et al. (ref. 4) data shown in figure 9 indicate significantly lower free-stream disturbance levels and also some spreading with Reynolds number beyond the peak. One can perhaps surmise the Reynolds number dependence of viscous superlayer effects in the Purtell data that are absent in the present results for high free-stream disturbance levels.

For the no-grid case (fig. 10), we do not have u_τ as a reference quantity. Plotted in figure 10 therefore is u'/u_e versus y/δ^*. The profiles fill out with distance downstream, but the peak values occur consistently at y/δ^* of about 1.2, very close to the location of $y/\delta^* = 1.33$ for which the low-frequency u' peak was observed in laminar flows at low free-stream turbulence levels by Klebanoff (ref. 7) and others. It would be of interest to see if the Klebanoff argument when applied to law-of-the-wall turbulent profiles explains the observed peak at $y^+ = 13$.

It is of interest at this point to look at disturbance spectra. Figure 11 shows spectra taken in the free stream 6 cm downstream of the leading edge of the plate for the three free-stream disturbance levels. Note the increase in intensity at the low frequencies with increase in turbulence level due to the grids. Inside the boundary layer, the spectra for grids 1 and 2 (figs. 12 and 13, respectively) are essentially unchanged with downstream distance at these high disturbance levels. For the no-grid case, however, there are progressive changes in the shape and intensity of the spectra (fig. 14). Although the intensities there are small, the largest growth rates occur in the frequency range 50 to 100 Hz (fig. 15), corresponding to $\beta\nu/u_e^2$ between 120×10^{-6} and 250×10^{-6}. It is premature to ascribe any linear instability connotations to this result.

SUMMARY

The foregoing is an interim report of our investigation. It is apparent that there is much yet to be done. One thing that is fairly clear is that no standard laminar flow was observed. Furthermore the turbulent mean flow data seem reasonable for the elevated disturbance levels of our tests in the sense that there is no discernible wake component to any of the profiles and that the variation of skin friction with Re_θ is consistent with zero wake strength. The no-grid data are in all likelihood transitional. This case requires additional concentrated study in order to obtain more definite information regarding the transition process in a disturbed environment.

REFERENCES

1. Musker, A.J.: Explicit Expression for the Smooth Wall Velocity Distribution in a Turbulent Boundary Layer. AIAA J., vol. 17, no. 6, June 1979, pp. 655-657.

2. Coles, D.E.: The Turbulent Boundary Layer in a Compressible Fluid, Rand Corp., Rep. R-403-PR, 1962.

3. Coles, D.E.: The Young Person's Guide to the Data. In Proceedings of 1968 AFOSR-IFP-Stanford Conf. (Vol. II), Stanford Univ., 1969, pp. 1-45.

4. Purtell, L.P.; Klebanoff, P.S.; and Buckley, F.T.: Turbulent Boundary Layer at Low Reynolds Number. Phys. Fluids, vol. 24, no. 5, May 1981, pp. 802-811.

5. Murlis, J.; Tsai, H.M.; and Bradshaw, P.: The Structure of Turbulent Boundary Layers at Low Reynolds Numbers. J. Fluid Mech., vol. 122, 1982, pp. 13-56.

6. Huffman, G.D.; and Bradshaw, P., A Note on von Karman's Constant in Low Reynolds Number Turbulent Flows. J. Fluid Mech., vol. 53, 1972, pp. 54-60.

7. Klebanoff, P.S.: Private communication.

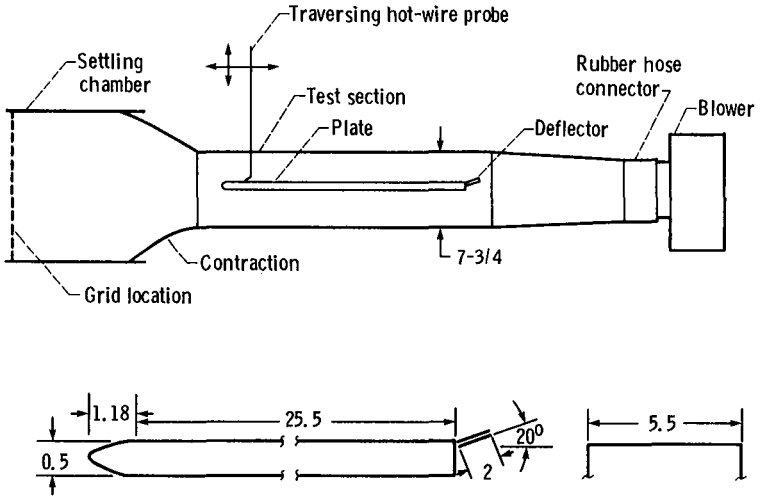

Figure 1. - Schematic diagrams of wind tunnel and test plate. (Dimensions are in inches.)

Grid	Dimensions, in				Open area, percent	u'_e/u_e, percent
	a	b	c	d		
1	1.75	1.50	2.25	1.75	33	5-6
2	1.38	1.75	1.25	2.00	24	6-7

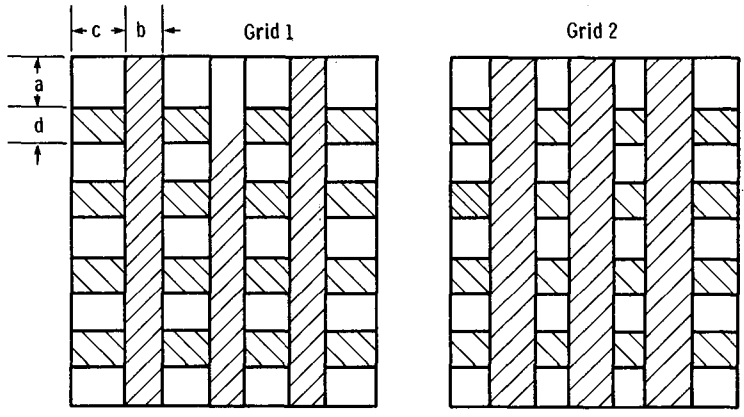

Figure 2. - Shapes and dimensions of grids.

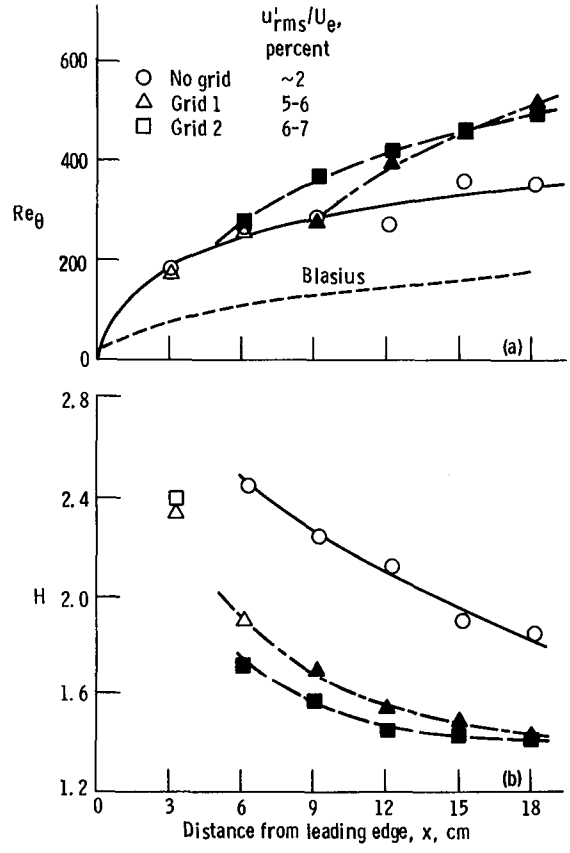

(a) Boundary-layer growth.
(b) Shape factor variation.

Figure 3. - Mean boundary-layer development.

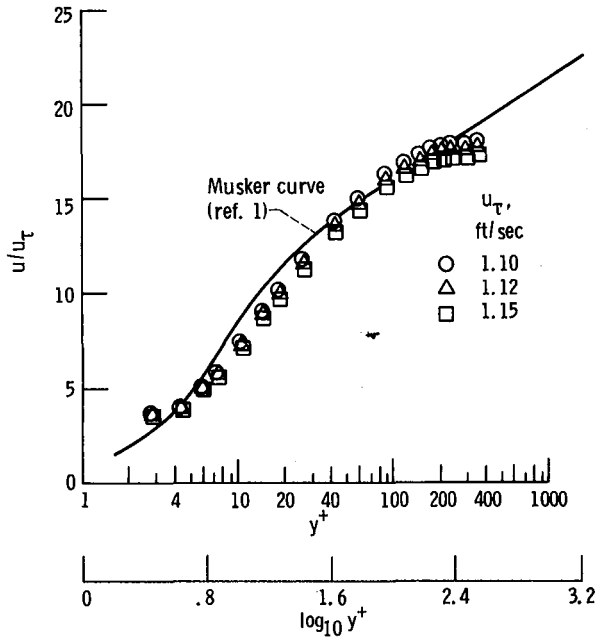

Figure 4. - Mean-velocity profile at 9 cm - grid 2. u_τ = 1.12 ft/sec.

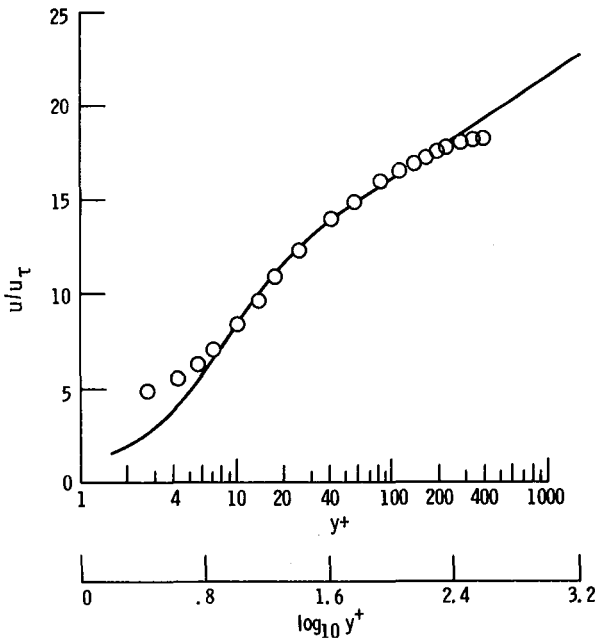

Figure 5. - Mean-velocity profile at 15 cm - grid 2. u_τ = 1.09 ft/sec.

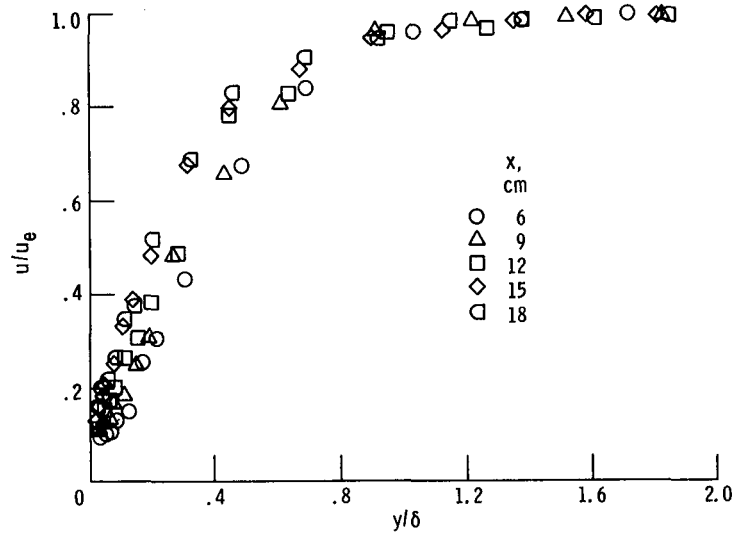

Figure 6. - Development of boundary layer - no grid.

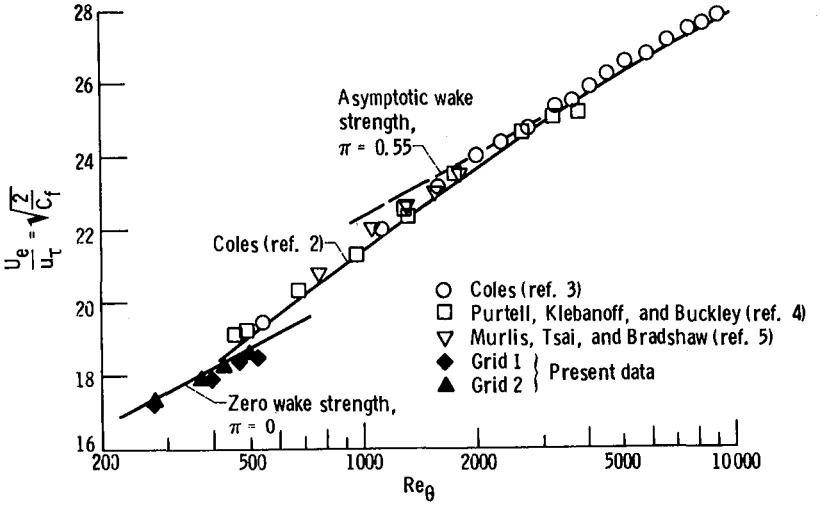

Figure 7. - Skin friction of turbulent boundary layers at low Reynolds numbers.

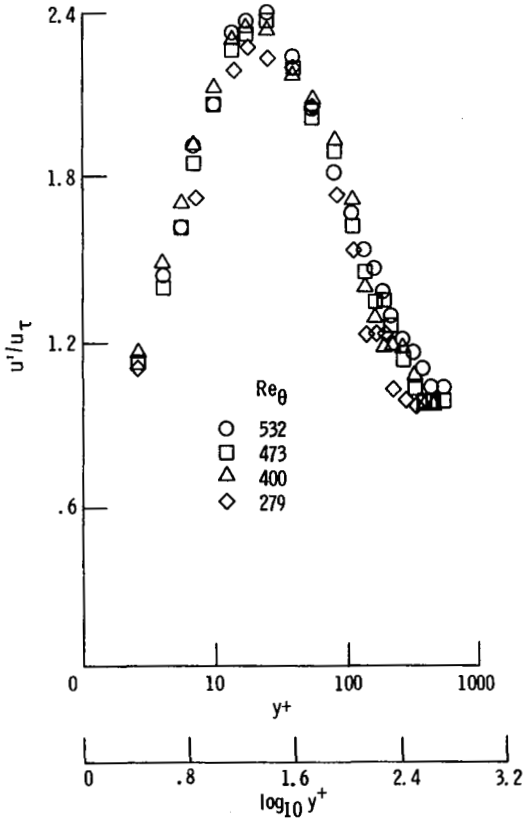

Figure 8. - Distribution of longitudinal fluctuating velocity - grid 1.

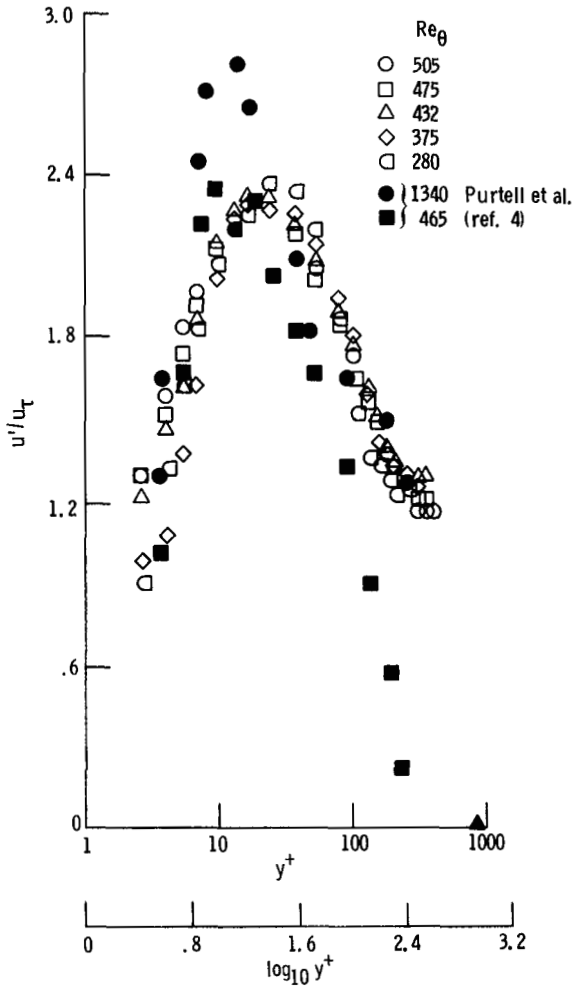

Figure 9. - Distribution of longitudinal fluctuating velocity - grid 2.

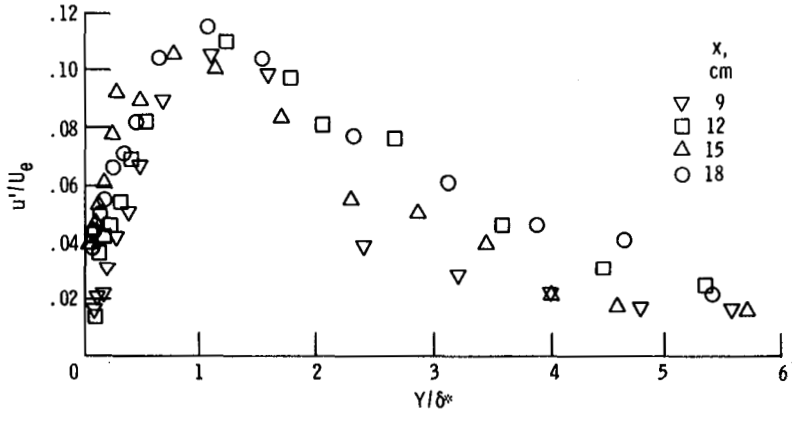

Figure 10. - Disturbance profiles for no-grid case.

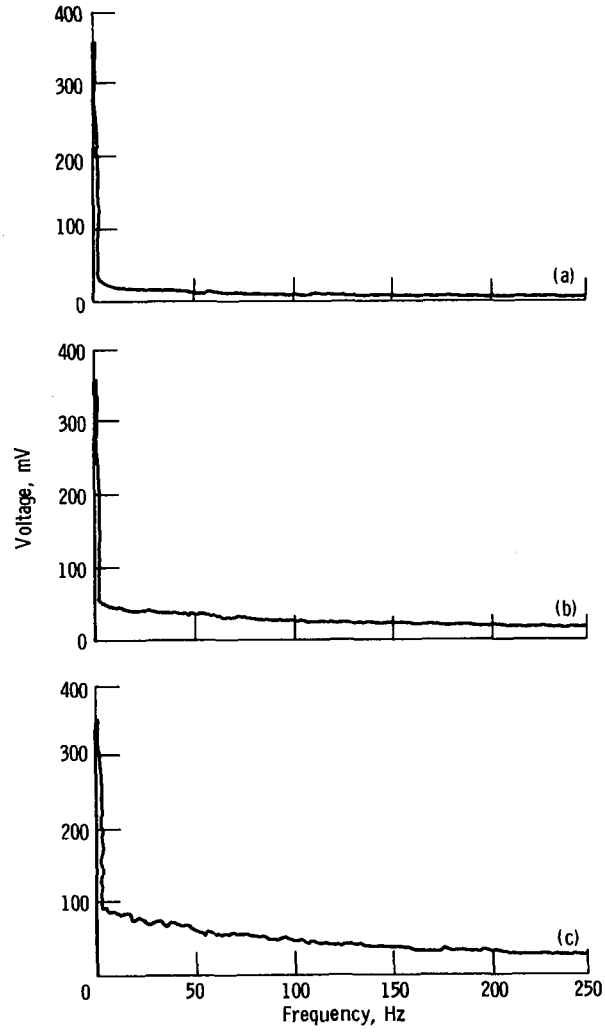

(a) No grid. (b) Grid 1. (c) Grid 2.

Figure 11. - Free-stream turbulence spectra, 0-250 Hz.

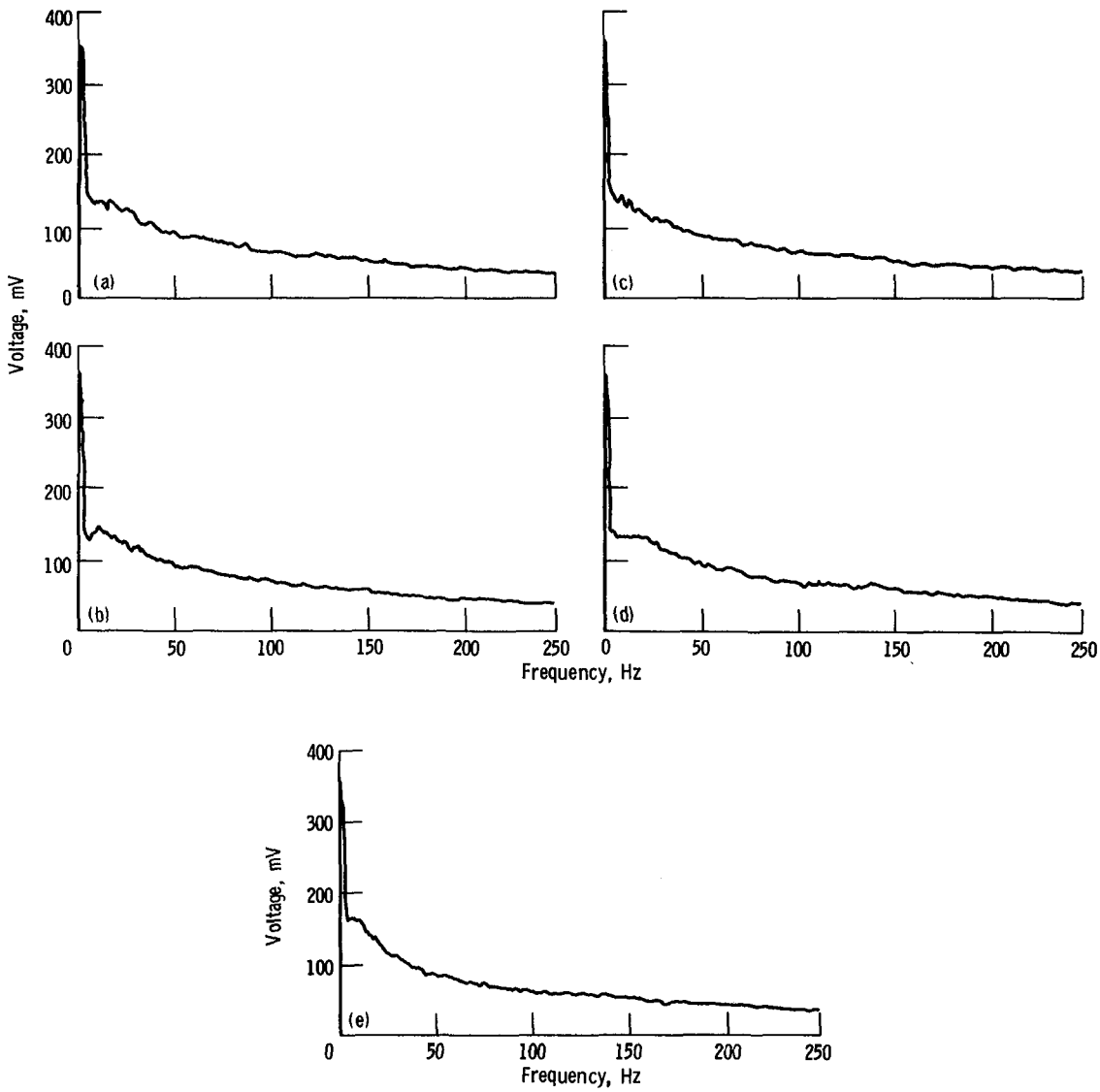

(a) x = 18 cm. (c) x = 12 cm.
(b) x = 15 cm. (d) x = 9 cm.
(e) x = 6 cm.

Figure 12. - Spectra of u' with increasing distance from leading edge - grid 1.

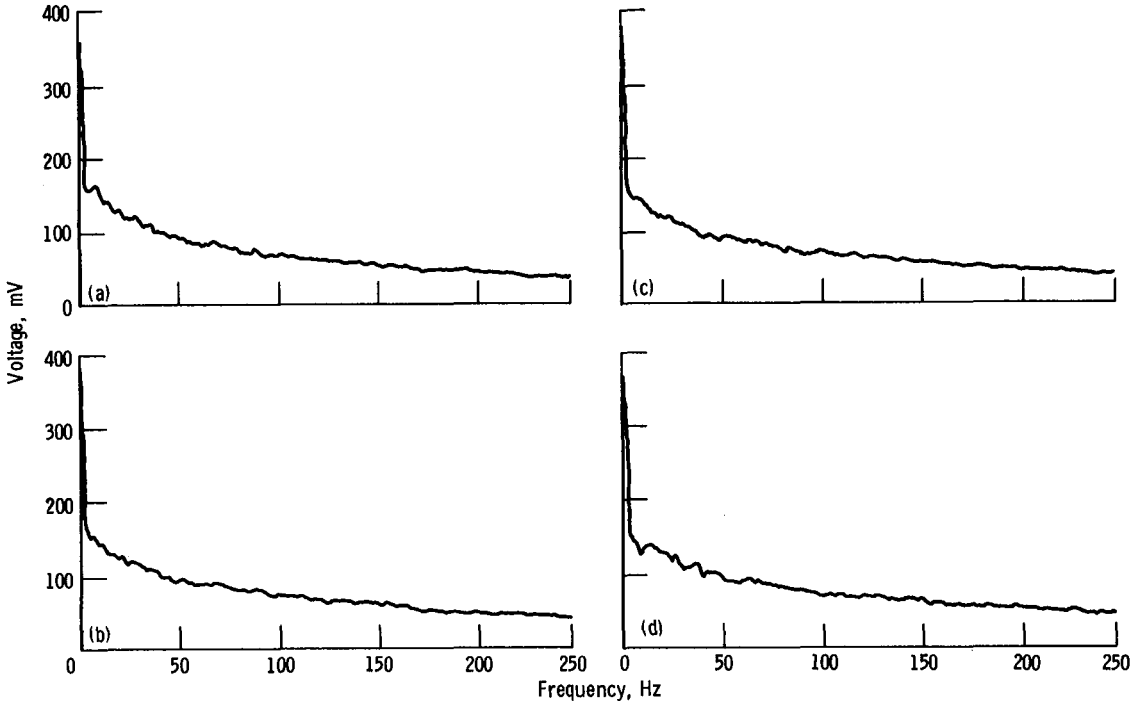

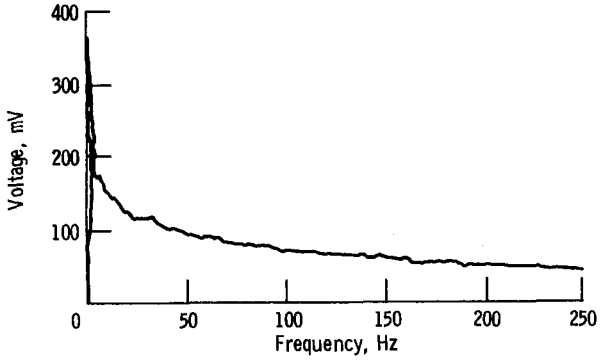

(a) x = 18 cm. (c) x = 12 cm.
(b) x = 15 cm. (d) x = 9 cm.
(e) x = 6 cm.

Figure 13. - Spectra of u' with increasing distance from leading edge - grid 2.

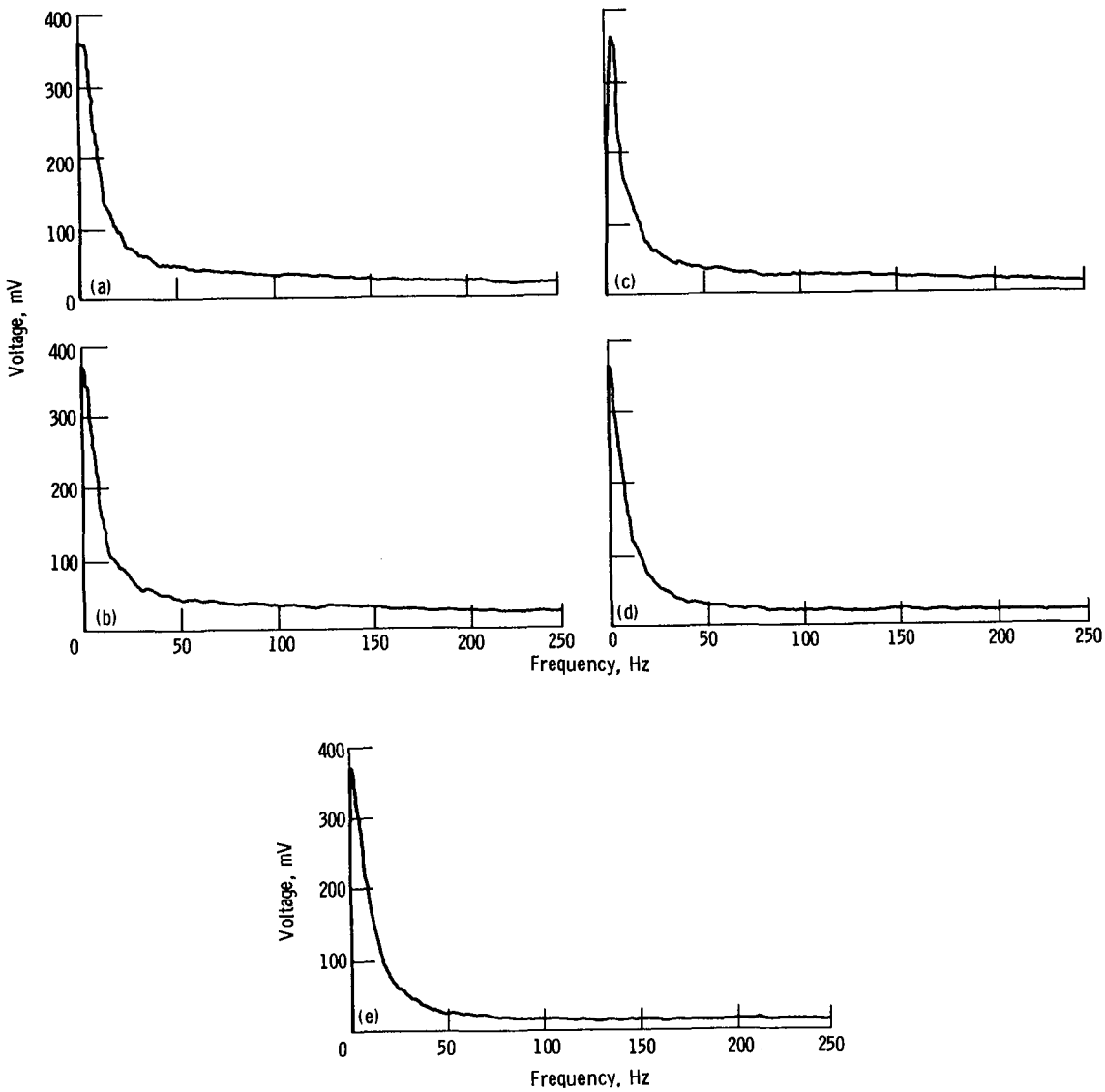

(a) x = 18 cm. (c) x = 12 cm.
(b) x = 15 cm. (d) x = 9 cm.
(e) x = 6 cm.

Figure 14. - Disturbance spectral data inside boundary layer - no grid.

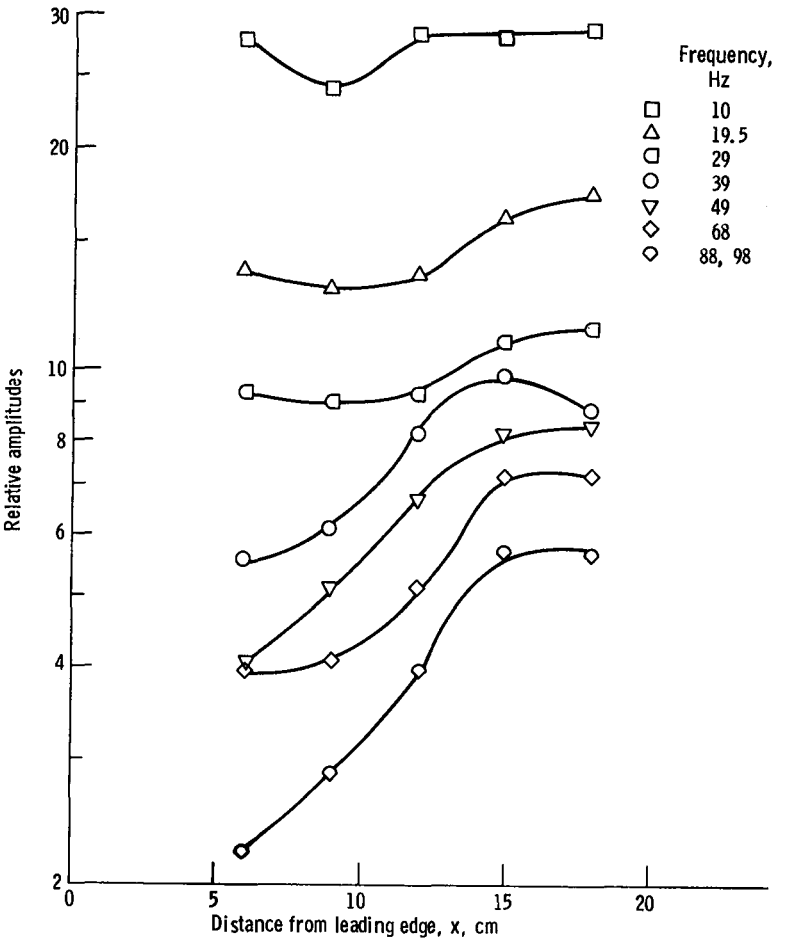

Figure 15. - Relative amplitudes of selected frequencies - no grid.